REGULAR PAPER

Engineering of optical, magneto-optical and magnetic properties of nickel-based one-dimensional magnetoplasmonic crystals

V. K. Belyaev[1*] , D. V. Murzin[1] , A. G. Kozlov[2] , A. A. Grunin[3], A. S. Samardak[2,4] , A. V. Ognev[2] , A. A. Fedyanin[3] , M. Inoue[5], and V. V. Rodionova[1]

[1]Immanuel Kant Baltic Federal University, Kaliningrad, 236041, Russia
[2]School of Natural Sciences, Far Eastern Federal University, Vladivostok, 690091, Russia
[3]Lomonosov Moscow State University, Moscow, 1199914, Russia
[4]National Research South Ural State University, Chelyabinsk, 4540805, Russia
[5]Toyohashi University of Technology, Toyohashi, 4418580, Japan

*E-mail: v.k.belyaev@gmail.com

Magnetoplasmonic crystals consisted of the combination of noble and ferromagnetic thin films deposited on diffraction gratings represent a special class of nanostructures that can utilize the magneto-optical Kerr effect enhanced by surface plasmon-polaritons excitation for the probing of an external DC magnetic field. Optical and magneto-optical properties of a magnetoplasmonic crystal are formed by magnetic behavior. This article represents ways to manipulate optical, magneto-optical and magnetic properties of nickel-based magnetoplasmonic crystals by the variation of the substrate parameters, the composition of magnetoplasmonic crystals as well as the compressive mechanical stresses on the surface of a ferromagnetic layer. © 2020 The Japan Society of Applied Physics

1. Introduction

In recent years, engineering of local and highly sensitive magnetic field sensors (MFSs) have become a rapidly developing topic due to the growth of accessibility of the nanostructures fabrication technologies. Nowadays, MFSs are applied in different areas of everyday life like medicine,[1,2] security systems,[3,4] touch emulation in robotics[5,6] and orientation devices.[7,8] Each area requires unique design specified to fulfill certain requirements and to determine the parameters of MFSs such as accuracy, energy efficiency, linear dimensions, locality and sensitivity. For this purpose, MFSs can be based on different physical phenomena[9,10] and the most widely used are induction coils, superconducting quantum interference devices[11,12] as well as Hall effect sensors,[13–15] sensors based on magneto-optical (MO) effects[16] and giant or tunnel magnetoresistance.[17–19] However, these sensors may require low temperatures, either lack the possibility to scan a certain area without moving a probe or have low sensitivity in local volumes. These disadvantages can be overcame by the use of the enhanced MO effects in magnetoplasmonic crystals (MPlCs).[20,21] MPlCs are periodically nanostructured ferromagnetic meta-surfaces that support the excitation and propagation of surface resonant evanescent wave coupled oscillations of metallic plasma and photons, called surface plasmon-polaritons (SPPs)[22,23] due to diffraction effects. The use of MPlCs allows one to enhance the value of MO effects in a narrow spectral region by two orders of magnitude and effectively use such type of nanostructures as a magnetic field probe that combines magneto-modulation and MO sensors techniques.[24,25] The main advantages of MPlC-based sensor are experimentally achieved high sensitivity of 10^{-6} Oe at a spot of 1 mm^2 and the possibility to scan an area without moving the magnetic field probe.[24,26–28]

The characteristics of the MPlC-based magnetic field probe are determined by the magnetic and MO properties: for effective use of MPlC-based MFSs, it is necessary to control the magnetic properties that determine the MO response, values of sensitivity, range of the detectable fields and required modulation field.[23] Magnetic properties of MPlCs can be tuned by the change of (i) the periodic modulation parameters,[27,29] that are responsible for forming the geometry driven magnetic anisotropy and the spectral position of MO effects enhancement; (ii) material and thickness of a ferromagnetic layer[30] that influence the values of magnetization and determine optical losses; (iii) the passivation layer thickness[31,32] for additional changes of mechanical stresses on top of a ferromagnetic layer.

The goal of this work is to demonstrate the influence of the variation of (i)–(iii) parameters on the MPlC-based magnetic field sensor's characteristics via magnetic and MO properties.

2. Experimental methods

MPlCs were fabricated by the DC ion-beam sputtering of metal and dielectric layers on the surface of smooth substrates made of silicon dioxide (Sub$_1$) and polymer with one-dimensional quasi-sinusoidal or trapezoidal shaped diffraction gratings (Sub$_2$ and Sub$_3$), respectively. Additional samples based on Sub$_1$ with a tape line on the surface were fabricated to estimate the thickness of deposited functional layers by the use of the NT-MDT Integra Aura atomic force microscopy (AFM) setup. The diffraction gratings on Sub$_2$ and Sub$_3$ have following declared parameters: period $d_2 = 320$ nm, $d_3 = 740$ nm and profile heights $h_2 = 20$ nm and $h_3 = 100$ nm. The substrates were covered with a layer of silver (Ag) or gold (Au) with the fixed thickness of 100 nm, a layer of nickel (Ni) with the thickness of 5, 20, 50 or 100 nm and a passivation layer of silica nitride (Si$_3$N$_4$) with the thickness of 20, 30 or 40 nm. Examples of AFM images and the surfaces' profiles extracted from the images for samples based on Sub$_2$ and Sub$_3$ are shown in Fig. 1.

The images show that d and h parameters have low deviation from declared values and the fabrication process did not affect the diffraction gratings shape. Short names of the samples, which describe the substrate type and the
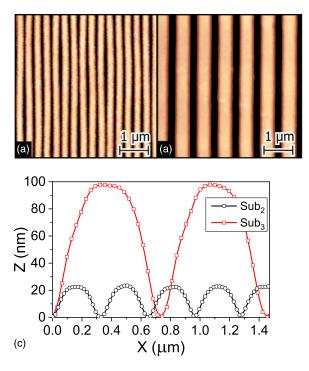
© 2020 The Japan Society of Applied Physics

Fig. 1. (Color online) Panels (a) and (b) demonstrate surface images of the MPlCs based on Sub_2 and Sub_3, respectively. Panel (c) represents the extracted surface profiles of the samples based on Sub_2 (black) and Sub_3 (red).

thickness of a ferromagnetic layer, will be used in this paper. For example, $Sub_1//Ag/Ni(100)$ means that it is the sample with following parameters and composition: $SiO_2//Ag(100\,nm)/Ni(100\,nm)/Si_3N_4(20\,nm)$. In case when the thickness of Si_3N_4 layer differs from 20 nm, it will be additionally mentioned.

Spectral and field dependences of optical and MO responses were studied by the setup consisting of a halogen lamp as a light source, a Glan–Taylor prism as a polarizer, a Hamamatsu H10722-20 photomultiplier tube with a monochromator and SR830 Lock-In amplifier as a detecting system accompanied by an optomechanical modulator and a system of Helmholtz coils which allow to control the modulation of light beam for measurements of optical and MO responses. All the measurements were carried out in the transverse magneto-optical Kerr effect (TMOKE) geometry using p-polarized light with the angle of incidence of 68°.[33] Frequencies of optomechanical and the AC magnetic field

modulation for optical and MO measurements were chosen to be 233 Hz and 317 Hz, respectively.

Integral and local magnetic properties of fabricated samples were measured with a LakeShore 7404i vibration sample magnetometer (VSM) and with a NanoMOKE II scanning laser magnetometer in the longitudinal magneto-optical Kerr effect geometry where the angle of incidence was set to 45° and the laser was focused into the spot of $10\,\mu m^2$. The sensitivity of integral and local magnetic properties measurements were 10^{-6} emu with the noise floor at 3 s/pt and 0.5 mdeg (rms) at 13 Hz rate, respectively. The VSM setup was additionally used to study the demagnetization processes in fabricated samples.

3. Results and discussion

3.1. Results

The tuning of the parameters of the MPlCs allows to vary optical and MO properties: the substrate type determines the shape and the spectral position of the diffraction gap and a narrow wavelength range of the TMOKE enhancement while the ferromagnetic layer thickness allows changing the values of optical losses and magnetization. In this measurements the TMOKE value was defined as $TMOKE = \Delta R(H)/R_0$, where R_0 is the reflection amplitude without magnetic field, which was detected by the optomechanical modulation of the incident light, and $\Delta R(H) = R_{+H} - R_{-H}$ denotes the field dependent reflection amplitude. All samples based on Sub_1 show no enhancement of the TMOKE in the visible light spectral region. Examples of the spectral dependences of reflectivity and the TMOKE values for the samples based on Sub_2 and Sub_3 are shown in Fig. 2.

Narrow spectral regions with clearly visible minima of reflectivity are related to the 1st and the 2nd diffraction orders for the MPlCs based on Sub_2 and Sub_3, respectively, and correspond to excitation of SPPs that cause the enhancement of the TMOKE response. An increase of the ferromagnetic layer thickness was followed by linear increase of optical losses and magnetization values, which corresponds to the decrease of reflectivity and the growth of the TMOKE value. To demonstrate the correlation between the MO and the magnetic properties, field dependences of TMOKE at the resonant wavelength, corresponding to the maximum of the TMOKE signal, were measured. These dependences were recalculated as a signal-to-noise ratio, $SNR_{AC} = \Delta R(H)/\sigma$,
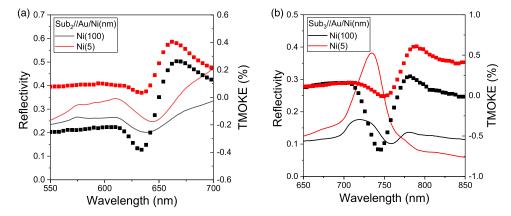

Fig. 2. (Color online) Spectral dependencies of reflectivity (solid lines) and TMOKE (squares) for MPlCs with different thickness of Ni layer based on (a) Sub_2 and (b) Sub_3.
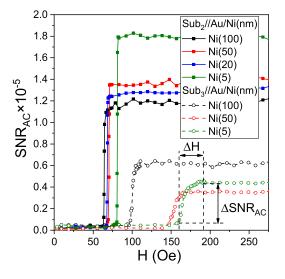
Fig. 3. (Color online) Field dependences of SNR_AC for MPlCs with the different thickness of Ni layer based on Sub_2 and Sub_3. ΔSNR_{AC} denotes the main drop of MO response in ΔH region.

where $\sigma = \sqrt{\sum_0^N (\Delta R_N - \overline{\Delta R})^2/(N-1)}$ is a standard deviation of noise measured at the same wavelength in the saturating magnetic field for $N = 500$ acquisition points. Examples of the SNR_{AC} field dependences are shown in Fig. 3.

The SNR_{AC} dependences have a step-like behavior where ΔSNR_{AC} value and ΔH region position depends on the magnetic properties and the optical losses in the ferromagnetic layer. ΔSNR_{AC} value determines the sensitivity and ΔH region shows the value of the necessary modulation field for proper work of the MPlC-based MFS.[26] To explain the behavior of $SNR_{AC}(H)$ dependences, the magnetic properties were studied.

All fabricated nanostructures based on Sub_1 have in-plane isotropic magnetic properties. The MPlCs based on Sub_2 and Sub_3 with diffraction gratings on the surface have geometry driven anisotropy of the magnetic properties with an easy magnetization axis (EMA) codirected with the stripes of diffraction gratings on the surface.[31,34,35] Magnetization processes along the EMA direction for all the samples are mostly determined by the domain wall movement that results in almost square loops.[24] Measurements of magnetic properties along the EMA direction correspond to the TMOKE geometry[26] and can be used to explain the field dependent MO response. The dependences of coercive force (H_c) along the EMA direction on the nickel layer thickness, the noble metal and the substrate types measured by local and integral methods are shown in Fig. 4.

Differences in local and integral magnetic properties for samples based on Sub_2 and Sub_3 can be explained by the features of used methods: local method allows one to study the magnetic properties in the central part of samples with a tightly focused laser beam, while the integral method is sensitive to the whole volume of a ferromagnetic material including edge defects[26] that are unavoidable due to the substrates fabrication method. Increased difference in magnetic properties for Sub_3-based samples can be caused by the diffuse reflection that starts to play an important role with the increase of d and h substrate parameters.[36]
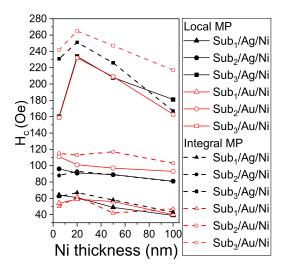

Fig. 4. (Color online) Dependences of H_c on nickel layer thickness, the noble metal (black for Ag and red for Au) and substrate types measured by integral (solid lines) and local (dashed lines) techniques.

Obtained dependences demonstrate the growth of H_c value with the appearance of surface modulation starting from samples based on Sub_1 to Sub_2 as well as the increase of the diffraction grating parameters d and h for the MPlCs based on Sub_2 to Sub_3. This tendency corresponds to the previous studies.[24] It can be explained by the inducement and enhancement of the geometry driven magnetic anisotropy: the presence of surface modulation leads to the formation of preferable magnetization direction, which is followed by the increase of H_c value for on Sub_2 and Sub_3 based MPlCs along the EMA direction.

The tendency of H_c value to increase with the reduce of the nickel layer thickness from 100 nm to 20 nm is in agreement with theoretical studies and can be explained by the replacement of a Bloch-type domain wall by Neel one at low thicknesses of the ferromagnetic layer.[37–40] The abrupt drop of H_c value for the Sub_3 based MPlCs with the nickel layer thickness of 5 nm can be explained by the appearance of discontinuities in the ferromagnetic layer caused by the difference of the ferromagnetic layer thickness and the h value of diffraction grating on the surface of Sub_3.[41]

Additionally, the possibility to tune magnetic properties by variation of the passivation layer thickness was studied. To
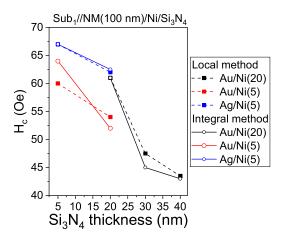

Fig. 5. (Color online) Dependences of H_c for different Si_3N_4 thickness measured by local (dashed lines) and integral (solid lines) methods.
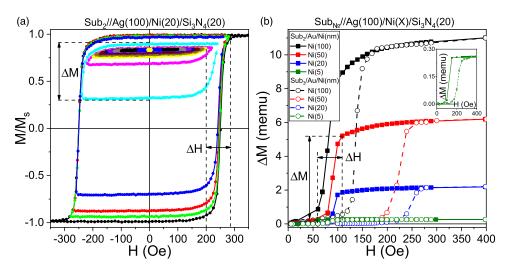
Fig. 6. (Color online) Panel (a) demonstrates an example of demagnetization process for MPlC with composition $Sub_2//Ag(100)/Ni(20)/Si_3N_4(20)$ and denotes the ΔM and ΔH values. Panel (b) shows the field dependences of the ΔM value for the MPlCs based on Sub_2 (solid lines) and Sub_3 (dashed lines).

neglect the influence of the edge defects the dependences of H_c value on the silicon nitride layer thickness for the Sub_1-based samples were studied. The collected data are shown in Fig. 5.

Determined dependences of H_c values on the Si_3N_4 thickness approve the possibility to tune the magnetic properties of fabricated samples by the change of mechanical stresses on top of ferromagnetic layer. Nickel has higher value of linear thermal expansion coefficients in respect to the silicon nitride. The increase of the silicon nitride layer thickness leads to the increase of compressive stresses on the interface with nickel layer which is followed by the decrease of the coercive force.[41,42]

Measurement technique for obtaining the field dependent MO response can be associated with the demagnetization processes in MPlCs. To demagnetize the samples, the following protocol was used: saturating magnetic field of $+H_{sat}$ applied along the EMA direction to the sample is alternately applied by $-H_{sat}$ in a positive and a negative direction, gradually decreasing and attenuating to zero. Due to the presence of the geometry driven magnetic anisotropy the samples were still difficult to demagnetize along the EMA and it was supposed to find the field range of ΔH, which is responsible for the main drop of the magnetic moment in the decreasing external field. To compare the demagnetization processes in different MPlCs the value of $\Delta M = M(+H) - M(-H)$ was calculated. The example of normalized magnetic moment of the magnetic field magnitude and the ΔM value on the substrate type and nickel layer thickness are shown in Fig. 6.

Collected data demonstrate that ΔH region occupies a field region starting at H_c field to zero field and its position strongly depend on H_c value. ΔH regions' positions and slopes defined by the demagnetization of the MPlCs correspond to the main region of the main drop of ΔSNR value that demonstrates the correlation of magnetic and MO properties. To use of MPlCs as the magnetic field probe there are two possible outcomes: (a) it is important to decrease necessary external modulation field that allows one to design compact sensor of the magnetic field and (b) the extension of ΔH region gives the possibility to probe magnetic fields at higher magnitudes. The (a) way can be

achieved by: decrease of diffraction gratings parameters d and h, increase of the ferromagnetic layer thickness and increase of the passivation layer thickness, while (b) way is just contrary to (a). The possibility to tune the position and the extension of ΔH region allows one to design and fabricate the MPlC with desirable parameters to fulfill the required values of sensitivity, accuracy, necessary modulation field and the value of maximum field to be measured.

4. Conclusions

The design and the functional layer parameters of MPlCs are fundamental in forming magnetic, optical and MO properties of the magnetic field probe based on the TMOKE enhanced by SPPs excitation. It was shown that by the variation of the MPlCs parameters it is possible to decrease the necessary external modulation field, to measure the magnetic fields of higher magnitudes and to precisely control the values of the TMOKE and the optical losses. The key parameters for such manipulation are the values of ΔM and ΔH region that can be tuned by: decrease of the substrates' diffraction grating parameters d and h, which is followed by the lowering of H_c value and narrowing ΔH range; increase of the ferromagnetic layer thickness, which is followed by the growth of the TMOKE value and the decrease of H_c and reflectivity values; increase of the passivation layer thickness that allows one to additionally lower H_c value. With approach, one can design and engineer the MPlCs that are able to fulfill desirable parameters for a required application or a specified task.

ORCID iDs

V. K. Belyaev ⓘ https://orcid.org/0000-0003-2772-3383
D. V. Murzin ⓘ https://orcid.org/0000-0002-5180-8873
A. G. Kozlov ⓘ https://orcid.org/0000-0001-8774-0631
A. S. Samardak ⓘ https://orcid.org/0000-0001-5917-4361
A. V. Ognev ⓘ https://orcid.org/0000-0002-1619-3666
A. A. Fedyanin ⓘ https://orcid.org/0000-0003-4708-6895
V. V. Rodionova ⓘ https://orcid.org/0000-0001-7793-538X

1) L. P. Ichkitidze, N. A. Bazaev, D. V. Telyshev, R. Y. Preobrazhensky, and M. L. Gavrushina, Biomed. Eng. **48**, 305309 (2015).
2) G. Lin., D. Makarov, and O. G. Schmidt, Lab Chip **17**, 1884 (2017).
3) P. Ripka, J. Phys.: Conf. Ser. **450**, 012001 (2013).
4) P. Nováček, J. Roháč, J. Šimánek, and P. Ripka, IEEE Trans. Magn. **49**, 6972 (2013).
5) S. Oh, Y. Jung, S. Kim, S. Kim, X. Xu, H. Lim, and C. Kim, Sci. Rep. **7**, 16963 (2017).
6) G. Boer, N. Raske, H. Wang, J. Kow, A. Alazmani, M. Ghajari, P. Culmer, and R. Hewson, Sensors **17**, 2539 (2017).
7) H. Park, J. Hwang, W. Choi, D. Shim, K. Na, and S. Choi, Sens. Actuators A **114**, 224 (2004).
8) L. Yan, B. Zhu, Z. Jiao, C.-Y. Chen, and I.-M. Chen, Sci. Rep. **4**, 06756 (2014).
9) P. Ripka, IEEE Sens. J. **10**, 11081116 (2010).
10) P. Ripka, K. Draxler, and R. Styblíková, Sensors **16**, 114 (2016).
11) R. L. Fagaly, Rev. Sci. Instrum. **77**, 101101 (2006).
12) M. José Martínez-Pérez and D. Koelle, Phys Sci. Rev **2**, 20175001 (2017).
13) T. Q. Hung, F. Terki, S. Kamara, K. Kim, S. Charar, and C. Kim, J. Appl. Phys. **117**, 154505 (2015).
14) A. Sandhu, A. Okamoto, I. Shibasaki, and A. Oral, Microelectron. Eng. **73–74**, 524 (2004).
15) B. Ozer, H. Piskin, and N. Akdogan, IEEE Sens. J. **19**, 5493 (2019).
16) M. Lindner and M. Koschny, Mater. Sci. Forum **170**, 1316 (2012).
17) M. Pannetir, C. Fermon, G. Legoff, J. Simola, E. Kerr, M. Welling, and R. J. Wijngaarden, IEEE Appl. Supercond. **15**, 892 (2005).
18) J. Zhang, Y. Wang, and J. Huang, Sensors **18**, 2881 (2018).
19) C. Zheng et al., IEEE Trans. Magn. **55**, 0800130 (2019).
20) A. A. Grunin, A. G. Zhdanov, A. A. Ezhov, E. A. Ganshina, and A. A. Fedyanin, Appl. Phys. Lett. **97**, 261908 (2010).
21) V. I. Belotelov, I. A. Akimov, M. Pohl, V. A. Kotov, S. Kasture, A. S. Vengurlekar, A. V. Gopal, D. R. Yakovlev, A. K. Zvezdin, and M. Bayer, Nat. Nanotechnol. **6**, 370376 (2011).
22) A. V. Zayats and I. I. Smolyaninov, J. Opt. A: Pure Appl. Opt. **5**, S16 (2003).
23) L. Novotny and B. Hecht, *Principles of Nano-Optics* (Cambridge University Press, Cambridge, 2012) 2nd ed., p. 377.
24) V. K. Belyaev, A. G. Kozlov, A. V. Ognev, A. S. Samardak, and V. V. Rodionova, J. Magn. Magn. **480**, 150153 (2019).
25) A. A. Grunin, I. R. Mukha, A. V. Chetvertukhin, and A. A. Fedyanin, J. Magn. Magn. Mater. **415**, 72 (2016).
26) V. K. Belyaev, D. V. Murzin, N. N. Perova, A. A. Grunin, A. A. Fedyanin, and V. V. Rodionova, J. Magn. Magn. **482**, 292295 (2019).
27) A. G. Kozlov, M. E. Stebliy, A. V. Ognev, A. S. Samardak, A. V. Davydenko, and L. A. Chebotkevich, J. Magn. Magn. **422**, 452457 (2017).
28) A. A. Grunin, A. V. Chetvertukhin, T. V. Dolgova, A. A. Ezhov, and A. A. Fedyanin, J. Appl. Phys. **113**, 17A946 (2013).
29) A. V. Davydenko, A. G. Kozlov, and L. A. Chebotkevich, J. Appl. Phys. **116**, 143901 (2014).
30) S. Ingvarssona, G. Xiaoa, S. Parkinb, and W. Gallagherc, J. Magn. Magn. Mater. **251**, 202 (2002).
31) A. E. Muslimova, A. V. Butashina, and V. M. Kanevskiia, Tech. Phys. Lett. **44**, 730 (2018).
32) G. G. Gumarov, A. V. Alekseev, and V. Y. Petukhov, J. Magn. Magn. Mater. **487**, 165322 (2019).
33) A. A. Grunin, N. A. Sapoletova, K. S. Napolskii, A. A. Eliseev, and A. A. Fedyanin, J. Appl. Phys. **111**, 07A948 (2012).
34) S. Ingvarssona, G. Xiaoa, S. S. P. Parkinb, and W. J. Gallagherc, J. Magn. Magn. Mater. **251**, 202 (2002).
35) V. Belyaev, V. Rodionova, K. Chichay, A. Grunin, and A. Fedyanin, Acta Phys. Pol. A **127**, 546 (2015).
36) D. Zook, Opt. Commun. **17**, 77 (1976).
37) M. S. Gabureac, L. Bernau, G. Boero, and I. Utke, IEEE Trans. Nanotechnol. **12**, 668 (2013).
38) S. V. Poliakov, B. I. Reznikov, A. V. Shchennikov, E. A. Kopytenko., and V. Samsonov, Seism. Instrum. **53**, 1 (2017).
39) Y. K. Kim and M. Oliveria, J. Appl. Phys. **74**, 1233 (1993).
40) C. T. Hsieh, J. Q. Liu, and J. T. Lue, Appl. Surf. Sci. **252**, 1899 (2005).
41) A. Bur, T. Wu, J. Hockel, C.-J. Hsu, H. K. D. Kim, T.-K. Chung, K. Wong, K. L. Wang, and G. P. Carman, J. Appl. Phys. **109**, 123903 (2011).
42) B. Zhu, C. C. H. Lo, S. J. Lee, and D. C. Jiles, J. Appl. Phys. **89**, 7009 (2001).